Finite element simulation of laser spot welding

A. De, S. K. Maiti, C. A. Walsh and H. K. D. H. Bhadeshia

The present work reports on a two-dimensional axisymmetric finite element analysis of heat flow during laser spot welding, taking into account the temperature dependence of the physical properties and latent heat of transformations. An analysis based on conduction heat transfer alone, but using the 'double ellipsoidal' representation of the laser beam, seems to be sufficient to estimate the transition to keyhole formation during laser spot welding, although the 'double ellipsoidal' representation requires an a priori knowledge of the expected weld pool dimensions. Transient temperature isotherms and the weld pool dimensions are predicted using the model; the latter are found to compare well with measurements of weld bead dimensions. The results show that the keyhole mode is stimulated using either a high laser power and low on-time or a low laser power and high on-time. The outcomes are found to be sensitive to the assumed absorptivity and the assumed weld pool depth used to define the 'double ellipsoidal' heat source. STWJ/362

Professor De and Professor Maiti are in the Mechanical Engineering Department, Indian Institute of Technology Bombay, Powai, Bombay 400 076, India (amit@me.iitb.ac.in). Dr Walsh and Professor Bhadeshia are in the Department of Materials Science and Metallurgy, University of Cambridge, Pembroke Street, Cambridge CB2 3QZ, UK. *Manuscript received 11 June 2002; accepted 8 November 2002.*

INTRODUCTION AND REVIEW

Laser heat sources are currently under active consideration in the development of alternative techniques for spot welding operations of the type frequently employed in the automobile industries. Laser beam welding has a number of desirable attributes. The heat affected zones are characteristically smaller and narrower than those produced using conventional welding techniques and distortion of the workpiece is reduced. They are also suitable for the welding of heat sensitive materials and, with appropriate selection of operating parameters, the same heat source can be used for both welding and cutting. As the mechanical properties of a weld are highly dependent on the cooling rate of the weld metal, a knowledge of the temperature field in and around the melt pool is essential for the understanding and modelling of the welding process. The present work is concerned with the calculation of the temperature field in and around the melt pool of laser spot welds and the prediction of the weld dimensions using a finite element model.

During laser spot welding, an intense beam is focused onto a small area. The material under the beam rapidly melts and may partly vaporise, leaving behind a small vapour filled crater, which enhances the absorptivity of the incident beam. This vapour filled crater is referred to as a 'keyhole'. The molten front extends more in the thickness than in the width direction if the laser power is sufficiently high. This can lead to a parallel sided molten pool and heat transfer occurs predominantly via radiative and convective modes through the vapour and molten material. When the laser power is low, however, the conduction mode of heat transfer dominates, resulting in a low depth to width ratio, low Péclet number, and failure to form a keyhole. The cooling rate in both instances depends on the laser power, weld dimensions, laser on-time, and absorptivity of the material to be welded. It is well known that the absorptivity depends on numerous material and process variables, leading to difficulties in predicting joint parameters.

Following the work of Rosenthal,[1] Swift-Hook and Gick[2] analytically modelled continuous laser welding assuming heat transfer by conduction only. The beam was represented as a moving line source with full penetration under all welding conditions. They[2] were able to estimate the weld dimensions as a function of laser power and beam velocity relative to the workpiece. Any discrepancy was attributed to the definition of the heat source and the failure to account for the convective heat flow. Andrews and Atthey[3] reported a three-dimensional heat transfer model, which assumed total absorption of power by the material as soon as the laser beam impinges on the workpiece. The keyhole dimensions were calculated considering convective flow in the weld pool to be driven by surface tension and gravity. The assumption regarding total absorption of the laser power is not realistic. Kaplan[4] calculated the keyhole profile using a point by point determination of the energy balance along the keyhole wall, locally solving the energy balance equation and representing the laser as a line heat source.

Pavelic *et al.*[5] introduced the concept of a distributed heat source with a Gaussian profile (Fig. 1) to represent a welding arc, in the form

$$q(r) = q_0 \exp(-Cr^2) \qquad (1)$$

where $q(r)$ is the heat flux at a radius r from the source centre, q_0 is the maximum heat flux, and C is an adjustable constant. Mazumder and Steen[6] presented the first numerical model for a continuous laser welding process using a

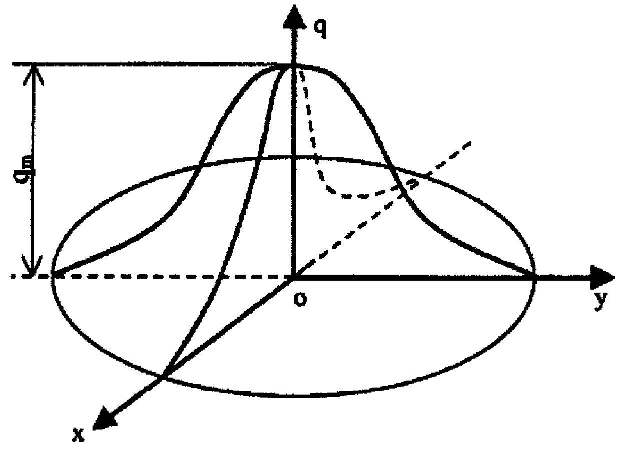

1 Gaussian distribution of heat intensity

DOI 10.1179/136217103225005570

Gaussian distribution for the moving laser beam. They assumed complete absorption of power above the boiling point and an absorption of 20% of the incident power below that temperature. The energy absorption was modelled according to the Beer–Lambert law $q_z = q_0 \exp(-\beta z)$, where β is the absorption coefficient and q_z and q_0 are the intensities at depth z and at the surface respectively. This model helped to simulate the physical phenomena leading to the formation of the keyhole. It was possible to predict the size and shape of the fusion zone and heat affected zone, and the temperature distribution in and around the joint.

Paul and DebRoy[7] reported a two-dimensional heat transfer model that considered both the conductive and convective heat transfer modes. They were also the first to include the convective heat transfer mode in the analysis, with a flow mechanism that was a function of the temperature dependence of the surface tension of the liquid pool.

Zacharia *et al.*[8,9] also developed a two-dimensional finite difference model using a Gaussian heat flux distribution to describe the convective heat transfer in the fusion zone during a pulsed laser welding process, including surface tension gradients and an absorptivity of 30%. It is not clear whether the same absorptivity was used once the material (or substrate) under the laser beam reached (and exceeded) its boiling temperature. The thermophysical properties were assumed to be temperature independent. Guo and Kar[10] developed a three-dimensional, analytical formulation for conduction mode, continuous laser beam welding for thin sheets. Although the latent heat was considered, the material properties were taken to be temperature independent.

The above review of previous investigations into numerical modelling of the laser beam welding process demonstrates that the consideration of the form of the laser beam in the actual analysis is an important issue. In the majority of studies, the laser beam power was considered to be sufficiently low, thereby limiting the application to conduction mode laser welding, i.e. low Péclet number and small depth of penetration, but this is not appropriate for high power lasers, which lead to keyhole formation and the transportation of heat well below the surface as soon as the laser beam impinges on the material. A Gaussian distribution of the laser beam, applied only on the top surface, is not adequate to describe this phenomenon. To overcome this limitation, a 'Gaussian rod' type volumetric heat source was proposed.[11] This comprises a Gaussian distribution of laser intensity above the surface and a uniform distribution extending down to a depth d_k into the material. This is useful for the modelling of welds having a very high depth to width ratio, e.g. parallel sided weld pools; however, a wide range of weld pool shapes is possible in reality depending on the process parameters, namely, laser power, welding speed, laser on-time, absorptivity, etc. It is necessary to consider how these variations can be accommodated in the analysis and to examine how a heat flux distribution can cater for both conduction and combined convection and conduction modes of heat transfer. This is the motivation for the present study.

Goldak and co-workers[12,13] then introduced a 'double ellipsoidal' type of representation of the welding arc in the context of fusion arc welding and also showed its suitability for modelling high penetration welding. The idea was a Gaussian input distribution over a 'double ellipsoidal' zone of dimensions $2a$, b, c_1, and c_2 ($c_1 < c_2$), as shown in Fig. 2. The heat input is explicitly given by

$$q(x,y,z,t) = \frac{6\sqrt{3} f_{1,2} Q}{abc_{1,2}\pi\sqrt{\pi}} \exp\left(-3\frac{x^2}{a^2}\right) \exp\left(-3\frac{y^2}{b^2}\right) \times \exp\left\{-3\frac{[z - v(\tau - t)]^2}{a^2}\right\} \quad . \quad . \quad . \quad . \quad (3)$$

where Q is the source intensity due to the heat source (i.e. welding arc, laser beam, electron beam, etc.), $2a$ represents the weld bead width, b is penetration, v is welding speed, c_1 and c_2 represent the extent of the heat source from its centre towards the front and rear of the source respectively (Fig. 2), and τ is defined as a time factor such that $t = 0$ and $v\tau$ is the distance between the heat source and the point of interest. This leads to a typical heat source that is a combination of two half ellipsoids – one in advance of the centre of the heat source and the other at the rear. The intensity of the source is distributed in a Gaussian manner within each half ellipsoid. The front ellipsoid is defined by a set of axes, namely, c_1, a, and b, whereas the rear ellipsoid is defined by c_2, a, and b. The constants f_1 and f_2 are associated with the front and rear section respectively and are related approximately by $f_1 + f_2 = 2$. The double ellipsoidal representation thus manifests a volumetric heat source and also considers the fact that for relative motion between the heat source and the material, there will be an asymmetry in the magnitude of the heat input between the front section and the rear section of the centre of the heat source. The only limitation of this representation[12,13] is that it requires a prior knowledge of the pool shape, i.e. parameters a, b, c_1, and c_2, which has somewhat restricted its generality. Mazumder *et al.* presented an extensive review of several efforts on modelling of laser beam processing.[14]

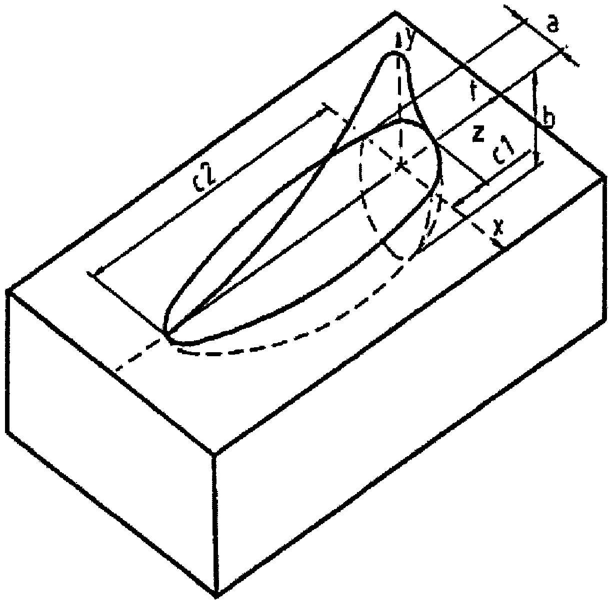

2 Double ellipsoidal representation of heat source

In 1999 Frewin and Scott[15] proposed a three-dimensional finite element analysis for pulsed laser welding. From experiments they found the heat flux distribution to be conical. The measured longitudinal power density distribution within the beam, as a function of distance from the focused spot, revealed the influence of the position of the focal point (with respect to the top surface) on the final weld bead dimensions. They considered in their study an extensive variation in the temperature dependent material properties but neglected convective heat flow within the molten pool. An excellent correlation was reported between the predicted and experimental weld bead dimensions.

The above brief review indicates that the form of the representation used for the laser beam has a significant effect on the results of numerical models of the laser beam welding process. A Gaussian representation of the laser beam, assuming heat input only on the top surface of the material, may not lead to correct results, especially for high power lasers that penetrate rapidly some distance into the material thickness, resulting in welds of high depth to width

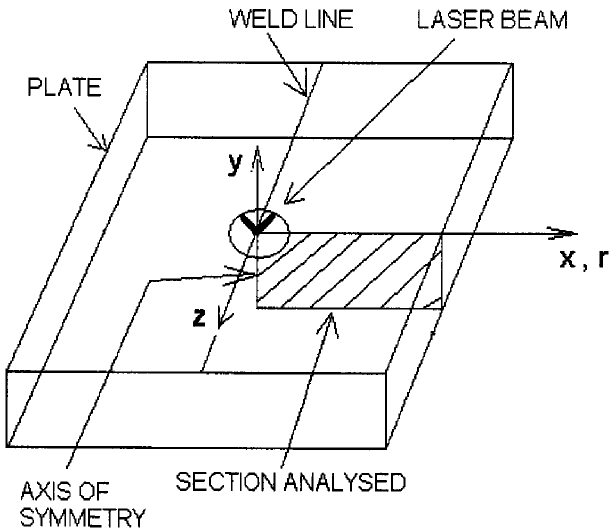

3 Transverse section considered for present analysis

ratio. The present work is thus aimed at a heat transfer analysis following the double ellipsoidal[12,13] representation of the laser beam, as this typically incorporates volumetric heat input from a heat source. The temperature dependence of the material properties, phase change phenomena, and convective and radiative heat losses from all the surfaces of a sheet are considered. The heat source being stationary in laser spot welding, the present work assumes a double ellipsoidal profile with $c_1 = c_2$, i.e. the extent of the beam is equal in both the front and the rear sections along the longitudinal direction. Although the parameter a is to be determined from the actual weld width,[12,13] in the present work $2a$ is considered to be equal to the focus diameter of the laser beam, as only the material directly beneath the beam will be subjected to direct heat input. Further, c_1 and c_2 are assumed to be equal to a, as the stationary beam is symmetric in both the longitudinal and transverse directions. An appropriate value of b is assumed, as will be explained below. The heat transfer analysis is therefore axisymmetric, with the y axis defined as the axis of symmetry (Fig. 3). The analysis is based on the finite element method and is used to make numerical estimates of weld bead dimensions for comparison with experimental data.

THEORETICAL FORMULATION

The governing equation of transient heat conduction in two-dimensional cylindrical coordinates is given by

$$\frac{1}{r}\frac{\partial}{\partial r}\left(rK\frac{\partial T}{\partial r}\right)+\frac{1}{r}\frac{\partial}{\partial y}\left(rK\frac{\partial T}{\partial y}\right)+\dot{Q}=sc\frac{\partial T}{\partial t} \quad (4)$$

where r and y are radial and axial coordinates, s, c, and K are density, specific heat, and thermal conductivity of the material respectively, T and t represent temperature and time respectively, and Q represents the rate of internal heat generation or input heat rate per unit volume. The values of K and c are considered to be temperature dependent. The essential and natural boundary conditions are expressed as

$$T = T_{S_1} \quad (5)$$

on the portion of the boundary S_1, and

$$K_n\frac{\partial T}{\partial n}-q+h(T-T_0)+\sigma\varepsilon(T^4-T_0^4)=0 \quad (6)$$

on the portion of the boundary S_2 and for $t>0$.

Incidentally, S_2 represents those surfaces that may be subject to radiation, convection, and imposed heat fluxes (q), K_n represents the thermal conductivity normal to the surface, T_0 the ambient temperature, h the convective heat transfer coefficient, ε the emissivity, and σ the Stefan–Boltzmann constant for radiation. Instead of considering the radiation term in the boundary condition, the effect of radiation and convection is considered together through a 'lumped' heat transfer coefficient[15] as $h = 2{\cdot}4\times10^{-3}\varepsilon T^{1{\cdot}61}$. Owing to the axial symmetry, the radial heat transfer across the laser beam axis (the symmetry line) is taken as zero, i.e. $\partial T/\partial r = 0$.

The governing equation (equation (4)) has been solved through finite element analysis. The final matrix equation to be solved is obtained in the following form

$$\left(\frac{2}{3}[\boldsymbol{H}]+\frac{1}{\Delta t}[\boldsymbol{S}]\right)(\{\boldsymbol{T}\})_{n+1}+\left(\frac{1}{3}[\boldsymbol{H}]+\frac{1}{\Delta t}[\boldsymbol{S}]\right)(\{\boldsymbol{T}\})_{n}+\frac{2}{\Delta t^2}\int_0^{\Delta t}\{f\}t\,\mathrm{d}t=0 \quad (7)$$

The elements of matrices [$\boldsymbol{H}$], [$\boldsymbol{S}$], and {f} are given by

$$h_{ij}^{e}=\iint\left(k\frac{\partial N_i}{\partial r}\frac{\partial N_j}{\partial r}+k\frac{\partial N_i}{\partial y}\frac{\partial N_j}{\partial y}\right)2\pi r\,\mathrm{d}r\,\mathrm{d}y \quad (8)$$

$$s_{ij}^{e}=\iint_V N_i scN_j 2\pi r\,\mathrm{d}r\,\mathrm{d}y \quad (9)$$

$$\{f^e\}=-\iint_V\left(\dot{Q}-sc\frac{\partial T}{\partial t}\right)N_i 2\pi r\,\mathrm{d}r\,\mathrm{d}y \quad (10)$$

where Δt is time increment and $\{\boldsymbol{T}\}_{n+1}$ and $\{\boldsymbol{T}\}_n$ are nodal temperature vectors corresponding to the $(n+1)$th and nth time steps respectively. The latent heat of melting and solidification is included in this simulation through an increase or decrease in the specific heat of the material. The specific heat c is expressed as follows

$$\left.\begin{array}{ll} c=C_1 & \text{for } T\leqslant T_S \\ c=C_2 & \text{for } T\geqslant T_L \\ c=C_m=\frac{\lambda}{T_L-T_S}+\frac{C_1+C_2}{2} & \text{for } T_S\leqslant T\leqslant T_L \end{array}\right\} \quad (11)$$

where λ is the latent heat (272·156 kJ kg^{-1}) and T_S (1480°C) and T_L (1540°C) are the solidus and liquidus temperatures respectively. During a phase change, the specific heat of an element is taken to be the weighted average of the associated specific heats; i.e. C_1 and C_m (for solid to mushy state or vice versa), C_m and C_2 (for mushy to liquid state or vice versa), or C_1, C_m, and C_2 (from solid to liquid state or vice versa).[16]

RESULTS AND DISCUSSION

The present theoretical study is based on measured geometric and material data for laser spot welds in a single sheet; the details are reported elsewhere.[17] The heat source was a JOLD 1000 diode laser with a laser beam spot diameter of 1·0 mm. It was focused using a lens of 50 mm focal length normally onto the top surface of a 2·0 mm thickness D52X low carbon steel sheet. The material composition is given in Table 1. Three levels of beam power, namely 1·0, 1·4, and 2·23 kW, and on-times varying in the range 0·15–2·65 s were considered, as presented in Table 2.

To model the results, a rectangular region of 15 mm (width) by 2 mm (thickness) is finely discretised (meshed) into divisions of 0·1 mm along the thickness direction. Along the width direction, a division of 0·1 mm is used up

Table 1 Chemical composition of workpiece material, wt-% (after Ref. 17)

C	Si	Mn	Cr	Mo	Ni	N	V
0·07	0·10	0·92	0·04	<0·01	0·03	0·005	<0·01

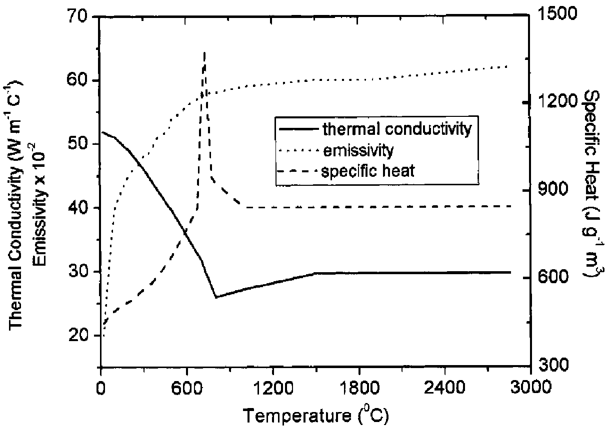

4 Temperature dependent physical properties of sheet material

to a distance of 5 mm, beyond which a division of 0·2 mm is used for the remainder of the length. A three node triangular ring type element is used.[16] The time span of the transient analysis includes the on-time of a single laser pulse and the subsequent cooling stage. The analysis is carried out through a number of small time steps, each time step being 0·001 s. Within each time step, a number of iterations is performed to achieve a convergence criterion of 1% (the difference in nodal temperature between two successive iterations). Figure 4 shows the temperature dependent material properties used in the calculations. During the analysis, whenever the temperature of a node exceeds the boiling point of the steel (2800°C), it is allowed to remain in the mesh at the boiling temperature and is not considered further in the analysis until cooling starts after removal of the laser beam. The volumetric heat input due to the laser is represented by adapting equation (4) for a stationary heat source, with $v=0$, $f=1{\cdot}0$, and $z=0$, giving

$$q(x,y)=\frac{6\sqrt{3}Q}{abc\pi\sqrt{\pi}}\exp\left(-3\frac{x^2}{a^2}\right)\exp\left(-3\frac{y^2}{b^2}\right) \qquad (12)$$

where Q is taken to be the incident laser power multiplied by the energy transfer efficiency (absorptivity). Among the three parameters a, b, and c ($c=c_1=c_2$ as described above) to be determined *a priori* for defining the double ellipsoidal profile of the laser beam, a and c are taken to be equal to the focal radius of the laser beam. In principle, $2a$ represents the weld width of the final weld bead and c the extent of the laser beam profile in the longitudinal direction.[12,13] However, instead of relying on some arbitrary approximation, it was decided to set both a and c equal to the focal radius of the beam. The parameter b, which in principle manifests the extent to which the beam penetrates below the top surface, is more problematic to decide *a priori.* A further complication is that the absorptivity of the laser beam is also a sensitive parameter in the modelling, as this directly controls the amount of heat input. In reality, the absorptivity depends on the substrate temperature and hence may vary with laser power and on-time as well as during the thermal cycle itself. Thus, in the present work, many numerical calculations were carried out for each combination of laser power and on-time (Table 2), using various

Table 2 Combinations of laser power and on-time examined

Laser power, kW	On-time, s					
1·0	0·15	0·65	1·15	1·65	2·15	2·65
1·4	0·15	0·65	1·15	1·65	2·15	2·65
2·23	0·15	0·165	0·180	0·195	0·210	0·225

values for b and the absorptivity, and the calculated weld bead dimensions were compared with the corresponding experimental results.[17] The best results were obtained with b equal to the sheet thickness (2·0 mm) for 1·4 and 2·23 kW and to 0·60 mm for 1·0 kW laser power. The absorptivity, at temperatures below the boiling point of the steel, was set to 50% for 1·4 and 2·23 kW laser powers, and 30% for 1·0 kW. There is no definite explanation for this change in absorptivity, but it was simply not possible to obtain the correct penetration at the higher powers using a value of 30%, given that b is the full thickness of the steel. It is speculated that the necessity for higher absorptivity values at higher powers occurs because the higher laser power densities lead to a rapid increase in the top surface and the weld pool temperatures, which possibly enhances the absorptivity.

In Fig. 5*a–c*, the maximum temperature isotherms for laser powers of 1·0, 1·4, and 2·23 kW respectively and an on-time of 0·15 s are compared with the corresponding weld pool shapes obtained experimentally. Since the steel studied melts at about 1500°C, the zone encompassed by the axis of symmetry and the 1500°C isotherm represents the molten zone or the weld pool. From these plots (Fig. 5), the weld width w and penetration p are estimated along the horizontal and vertical direction respectively. The position of the weld pool boundary in the experimental weld cross-sections was assessed from the grain structure and is depicted as a white line in Figs. 5–7. A comparison of Fig. 5*a* and *b* shows that the weld dimensions do not change significantly as the laser power is increased from 1·0 to 1·4 kW for an on-time 0·15 s. In contrast, an increase in laser power to 2·23 kW (Fig. 5*c*) shows a marked increase in penetration from approximately 0·5 mm (both at 1·0 and at 1·4 kW) to 1·4 mm (at 2·23 kW). The weld pools corresponding to laser powers of 1·0 and 1·4 kW (0·15 s on-time) are nearly semicircular (Fig. 5*a* and *b*), which is typical of conduction mode welding, but for a power of 2·23 kW the penetration increases substantially in comparison with the weld width. This is further evident as the on-time is increased from 0·15 to 0·21 s at 2·23 kW laser power (Fig. 6); the isotherms become almost parallel to the laser beam axis in the lower half of the weld, resulting in an almost nailhead like shape of the molten zone and a higher penetration to weld width ratio. A similar situation is also observed for a laser power of 1·4 kW and on-time of 2·65 s (Fig. 7), although the penetration to weld width ratio is lower in comparison with Fig. 6. The experimentally obtained weld pool shapes shown in Figs. 6 and 7 confirm the numerical calculations and also, typically, indicate a strong presence of the keyhole mode of heat transfer, i.e. immediate transport of heat inside the material volume as the beam impinges on the substrate. All the calculated weld pool shapes shown in Figs. 5–7 are similar to the experimentally measured weld pool shapes. Although not reported for all the combinations of laser power and on-time (Table 2), similar agreement was also obtained for the other cases. The experimental weld pool shapes in Figs. 6 and 7 show a crater at the top evidencing loss of material, possibly due to excessive vaporisation when total energy input (laser power × on-time) is too high: this, however, cannot be predicted through the computations since analysis of the vapour phase is not considered.

Figure 8 shows the variation in weld bead aspect ratio w/p obtained from the calculated weld bead dimensions. At 1·0 kW laser power, w/p remains nearly constant after a small decrease above 0·15 s. Similar variations are observed for 1·4 kW laser power, but in general the aspect ratios are lower compared with those for a 1·0 kW laser power. However, the ratio w/p decreases rapidly at 2·23 kW even for a small increment in on-time (from 0·15 to 0·225 s), strongly indicating the significance of a volumetric heat input to the material well below the top surface. This

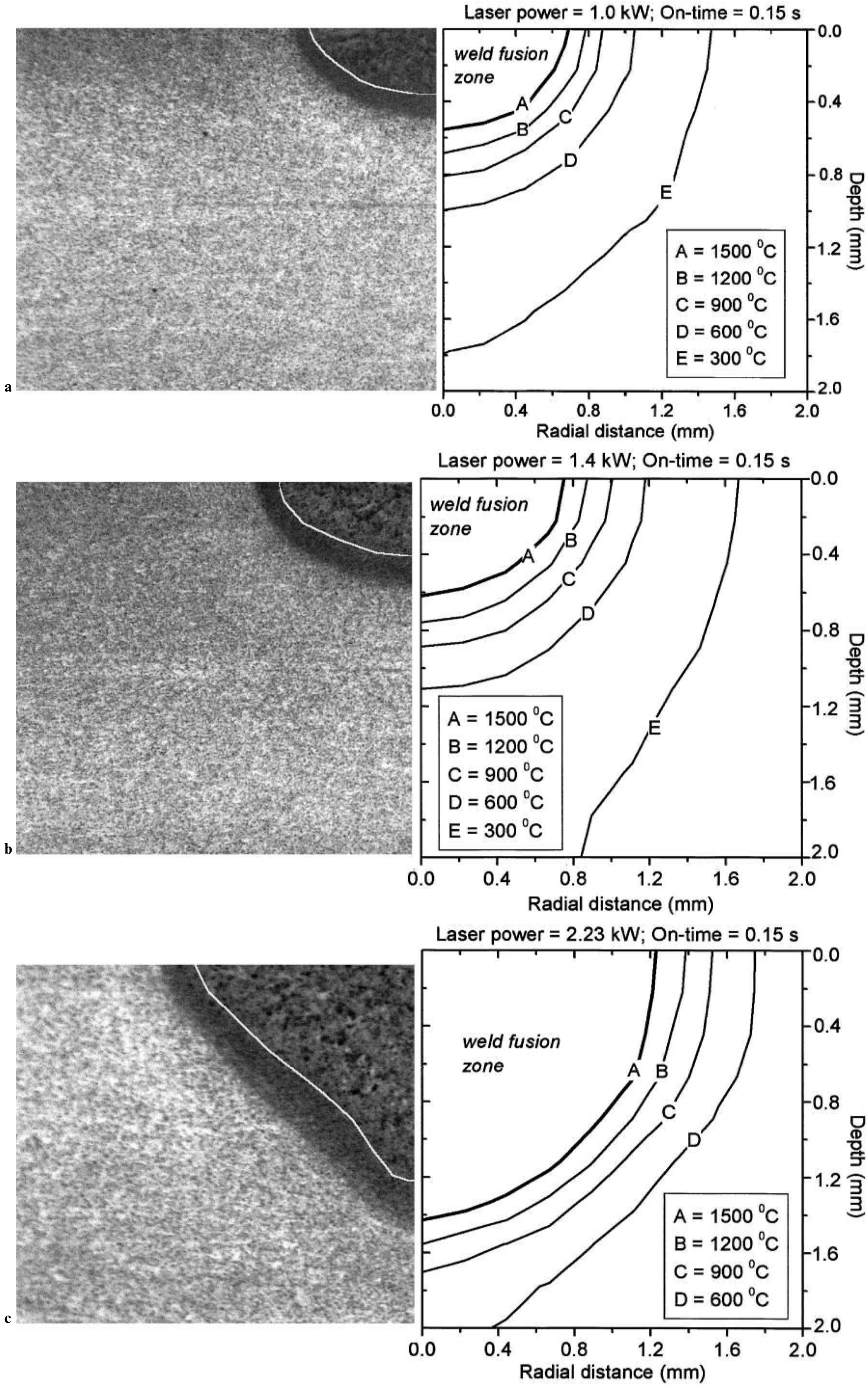

5 Comparison of experimental (left) and computed (right) fusion zone for on-time of 0·15 s and laser power of *a* 1·0, *b* 1·4, and *c* 2·23 kW

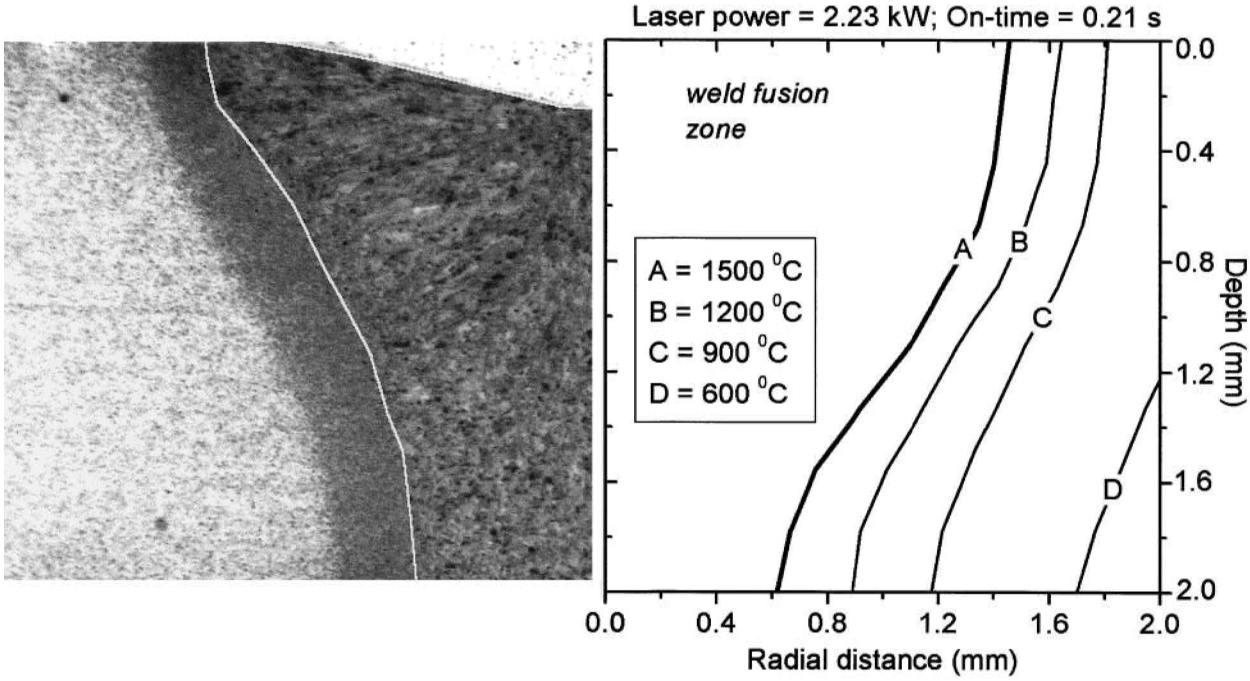

6 Comparison of experimental (left) and computed (right) fusion zone for laser power of 2·23 kW and laser on-time of 0·21 s

indirectly indicates the dominance of the keyhole mode of heat transfer in reality, through the metal vapour present inside the keyhole, i.e. the vapour phase present in the developing weld pool.

Figure 9*a–c* shows the variation of the computed weld width and penetration with on-time for 1·0, 1·4, and 2·23 kW laser powers respectively. At 1·4 kW laser power, full penetration is achieved for an on-time of 2·15 s (Fig. 9*b*); a further increase in on-time is therefore unnecessary. For 2·23 kW laser power, this occurs at an on-time of 0·21 s (Fig. 9*c*). Over the range of variables considered in the present work, the difference between the computed weld width and penetration, normalised with respect to sheet thickness t (i.e. $(w-p)/t$) is plotted versus on-time for the different laser powers (Fig. 10). Although an overall linear variation is evident, Fig. 10 also highlights the effects of laser power and on-time on weld shape. At the highest laser power (2·23 kW), increasing the on-time results in a much greater increase in penetration than in width, until full penetration is reached at 0·21 s. A similar variation is also observed for 1·4 kW laser power, but only for the lowest on-times. After 0·65 s the width and

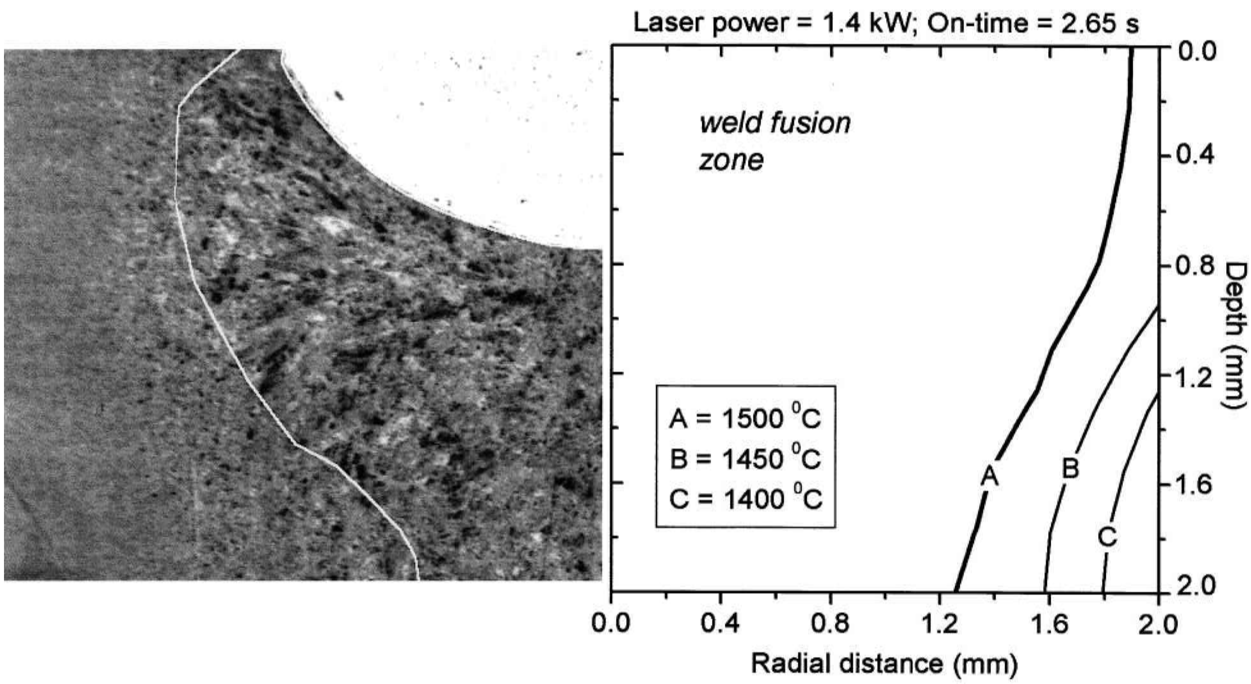

7 Comparison of experimental (left) and computed (right) fusion zone at laser power of 1·4 kW and laser on-time of 2·65 s

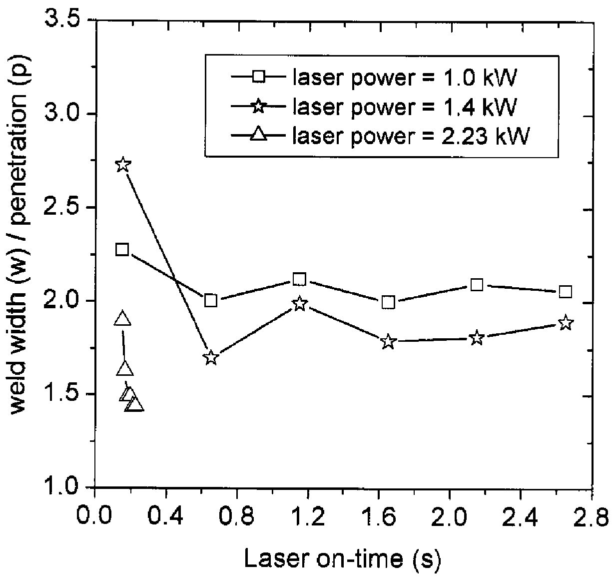

8 Variation of weld pool aspect ratio with on-time for three laser power values examined

penetration increase approximately proportionately (Fig. 9*b*) until full penetration occurs at 2·15 s. At the lowest power (1·0 kW) a proportionate increase in width and penetration occurs throughout the range of on-times considered; no significant change in weld shape occurs. The shape changes predicted for low on-times at the higher powers are undoubtedly associated with keyhole formation and the transition from conduction mode to keyhole mode welding.

The variation of total energy, i.e. laser power × on-time, with a parametric combination w^2p, related to calculated weld pool volume, is shown for the three laser powers in Fig. 11. The relationship is almost linear. Since w^2p is related to the volume of the molten metal in the weld pool, the total energy supplied directly influences the weld pool size.

It has been attempted in the present work to optimise the heat source parameter b and absorptivity by comparing the computed results with experimental data for laser spot welding. In conjunction with the double ellipsoidal parameters a and c, the parameter b determines the number of finite elements receiving direct heat input from the start of the computation. At low powers, e.g. 1·0 kW, the experimentally obtained penetration varies only from 0·39 mm at 0·15 s to 1·27 mm at 2·65 s. During the computations, it was observed that an initial setting of b=0·60 mm consistently produced the most accurate predictions. For an absorptivity of 30%, the results improved for low on-times when b was reduced by 20%, but for higher on-times the weld pool predictions deteriorated. This deterioration was reversed when b was increased by 20%. At 2·23 kW power, the calculations were observed to be less sensitive to the changes in the initial setting of b. It was found, however, that even with b set to the complete sheet thickness (2·0 mm), it was not possible to obtain satisfactory results without increasing the absorptivity to 50%, for which the computed weld dimensions showed the best agreement with the experimental data (Fig. 9*c*). A similar situation was observed for 1·4 kW power, especially for on-times greater than 1·15 s, whereas for 1·0 kW power the results were sensitive to the initial setting of b for on-times less than or equal to 1·15 s. Although it is conceivable that the absorptivity does indeed increase with increasing power density, this apparent change in absorptivity could also be related to the changes in the weld

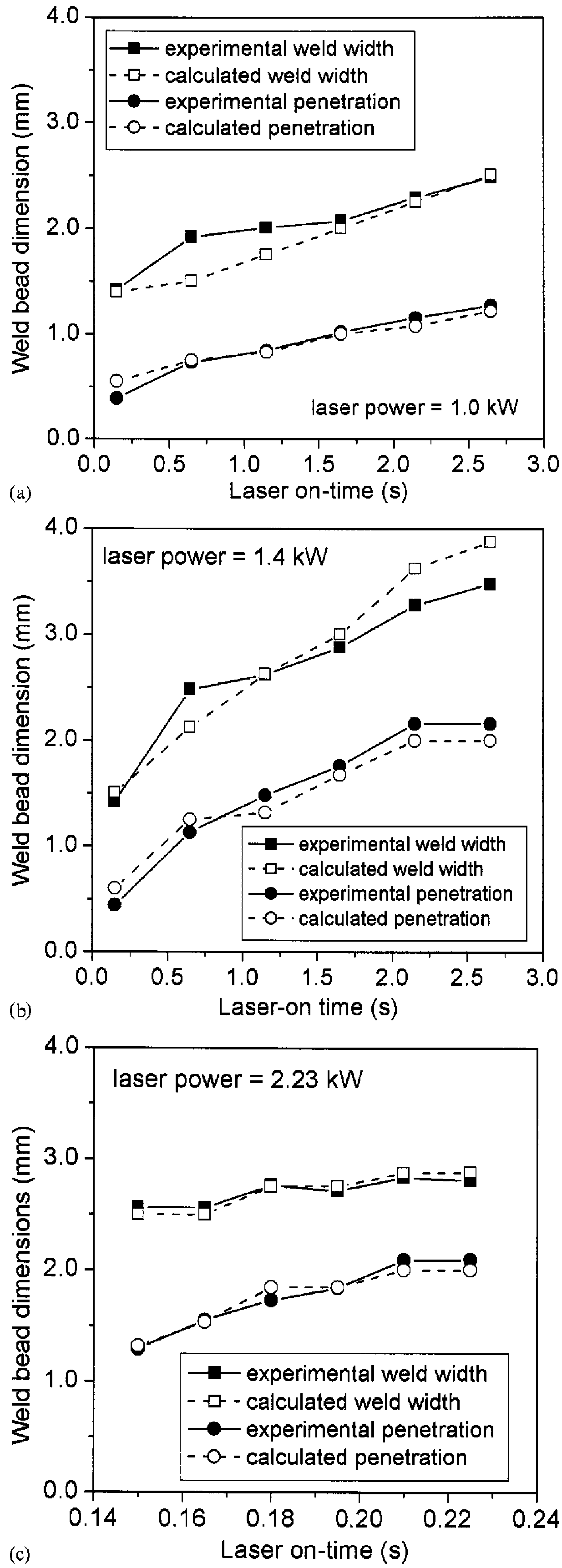

9 Comparison of calculated results with experimental data[17] for laser power of *a* 1·0, *b* 1·4, and *c* 2·23 kW

pool dimensions, temperature of the weld pool surface immediately under the beam, heat conduction, and the heat convection within the melt pool. For situations dominated

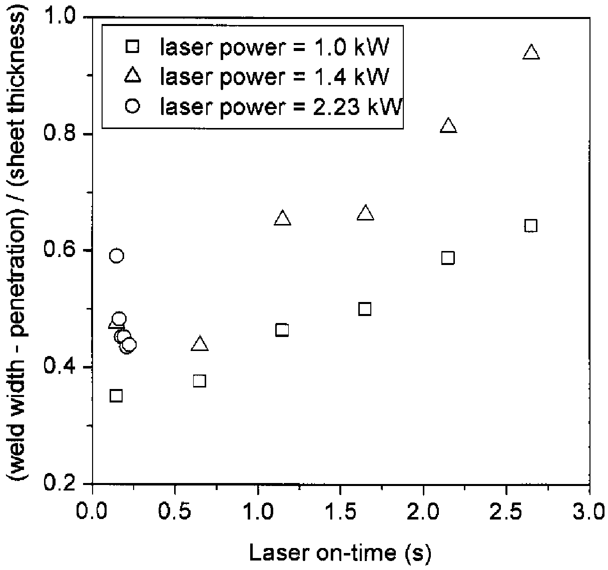

10 Variation of dimensionless difference between weld width and penetration with laser on-time for three laser power values examined

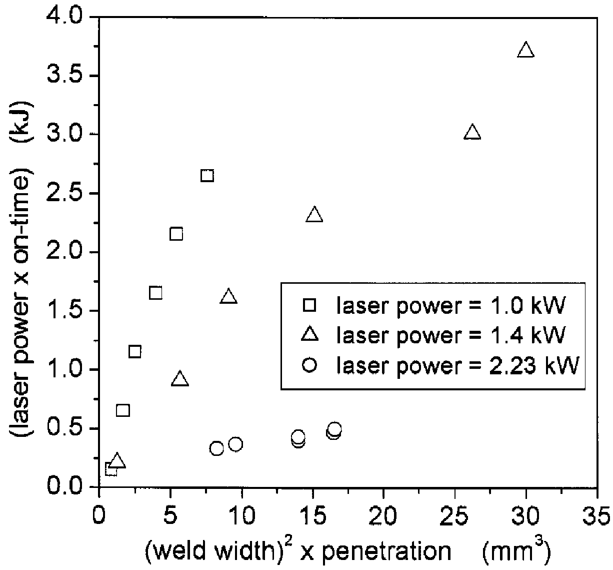

11 Variation of supplied laser energy with weld pool volume parameter combination for three laser power values examined

by the keyhole mode of heat transfer (i.e. at 2·23 kW laser power), the absorptivity used in the present study is nevertheless found to be highly effective and is recommended.

CONCLUSIONS

An analysis based on conduction heat transfer alone, but using the 'double ellipsoidal' approximation to the laser beam, seems to be sufficient for estimating the transition to keyhole formation, i.e. weld pools having high penetration to width ratio, during laser spot welding. To accomplish this, values must be set for two parameters, the first being b, associated with the double ellipsoidal heat source, and the second being the absorptivity. For higher power densities the most accurate results are obtained when b is equal to the complete sheet thickness, whereas at low power densities its value must be determined by comparison with an experimental weld. The absorptivity appears to be a function of the laser power, which can be indirectly related to the weld pool temperature. It is a somewhat intractable task to establish experimentally the relationship between absorptivity and laser power or temperature for a wide range of laser and material combinations, and it has instead been found effective to assign a single absorptivity value depending on laser power density as followed in the present work.

Using this method, it has been possible to estimate fairly accurately the weld pool dimensions, including the transition from conduction to keyhole modes, as a function of laser power and on-time for a variety of published experimental data.

ACKNOWLEDGEMENTS

The authors wish to acknowledge the financial support provided by the British Council, UK and the Department of Science & Technology, India under the scheme of UISTRF (UK – India Science and Technology Research Fund). One of the authors (CAW) would like to thank ABB AG, Germany for financial support and for the weld samples.

REFERENCES

1. D. ROSENTHAL: *Trans. ASME*, 1946, **68**, 849–865.
2. D. E. SWIFT-HOOK and A. E. F. GICK: *Weld. J.*, 1973, **52**, (11), 492s–499s.
3. G. J. ANDREWS and D. R. ATTHEY: *J. Phys. D, Appl. Phys.*, 1976, **9**, (15), 2181–2194.
4. A. KAPLAN: *J. Phys. D, Appl. Phys.*, 1994, **27**, (9), 1805–1814.
5. V. PAVELIC, R. TANBAKUCHI, O. A. UYEHARA and P. S. MYERS: *Weld. J.*, 1969, **48**, (6), 295s–305s.
6. J. MAZUMDER and W. M. STEEN: *J. Appl. Phys.*, 1980, **51**, (2), 941–947.
7. A. PAUL and T. DEBROY: *Metall. Trans. B*, 1988, **19B**, 851–858.
8. T. ZACHARIA, S. A. DAVID, J. M. VITEK and T. DEBROY: *Metall. Trans. A*, 1989, **20A**, 957–967.
9. T. ZACHARIA, S. A. DAVID, J. M. VITEK and T. DEBROY: *Weld. J.*, 1989, **68**, (12), 499s–509s.
10. W. GUO and A. KAR: *Sci. Technol. Weld. Joining*, 2000, **5**, (5), 317–323.
11. W. S. CHANG and S. J. NA: *J. Mater. Process. Technol.*, 2002, **120**, 208–214.
12. J. GOLDAK, A. P. CHAKRAVARTI and M. BIBBY: *Metall. Trans. B*, 1984, **15B**, 229–305.
13. J. GOLDAK, M. BIBBY, J. MOORE, R. HOUSE and B. PATIL: *Metall. Trans. B*, 1986, **17B**, 587–600.
14. J. MAZUMDER, P. S. MOHANTY and A. KAR: *J. Mater. Product Technol.*, 1996, **11**, (3/4), 193–251.
15. M. R. FREWIN and D. A. SCOTT: *Weld. J.*, **1999**, (1), 15s–22s.
16. A. DE: *Sci. Technol. Weld. Joining*, 2002, **7**, (2), 119–124.
17. C. A. WALSH, H. K. D. H. BHADESHIA, A. LAU, B. MATTHIAS, R. OESTERLEIN and J. DRECHSEL: *J. Laser Appl.*, 2003, **15**, (2), 68–76.